Journal of Theoretical and Applied Mechanics, Sofia, Vol.53 (2023) pp. 389-403
FLUID MECHANICS

MODELLING OF POLYMER FLOW INSTABILITIES WITH APPLICATION TO 3D PRINTING

SONIA TABAKOVA*, RUMIANA KOTSILKOVA

Institute of Mechanics, Bulgarian Academy of Sciences,
Acad. G. Bonchev Str. Bl.4, 1113 Sofia, Bulgaria

[Received: 12 August 2023. Accepted: 5 October 2023]

doi: https://doi.org/10.55787/jtams.23.53.4.389

ABSTRACT: Complex flow instabilities including wall slip and shear banding occur in many industrial applications, such as in polymer extrusion processes, thus affecting the throughput and the quality of the final product. The modelling of rheological data is a key point when studying different polymeric flows. The present survey incorporates three different ways to model the shear stress of shear thinning polymers as nonlinear functions of shear stress: generalized Newtonian model (Carreau-Yasuda model), wall shear slipping and banding with yield (Herschel–Bulkley model). Based on these models, the flow in the nozzle tube of a 3D printer is analyzed by a numerical model and two analytical models: the classical Weissenberg–Rabinowitsch–Mooney (WRM) model with slip; a simple model in three different regions in the tube (including yield, parabolic and band, which match their boundaries). The real data of measured shear stress by a plate–plate rheometer for three nanocomposites is used to compare the three models. The experimentally measured flow rates during the extrusion of the same nanocomposites are used to give insight into the corresponding flow structures in the nozzle tube.

KEY WORDS: shear thinning nanocomposites, shear inhomogeneity, wall slip, shear banding, flow in a tube.

1 INTRODUCTION

The mechanical behaviour of complex fluids such as polymer melts and concentrated polymer solutions is a subject of nonlinear polymer rheology. The rich phenomenology of complex fluids includes flow instabilities, resulting in heterogeneous "shear banded" states that display oscillations or irregular fluctuations [1,2]. Shear banding, either steady or transient, is now well-established in a variety of soft materials, including worm-like micelles, liquid crystals, entangled polymer solutions and melts,

*Corresponding author e-mail: stabakova@gmail.com

yield stress fluids, colloidal suspensions, etc. [3–6]. Particularly, in polymeric materials, shear banding is a phenomenon whereby regions of different shear rates, called "bands," can coexist in a system with sharp interfaces between them; for example, liquid-like bands flow to a solid-like region or a highly aligned phase adjacent to a less aligned one [4]. A limited number of publications discussed the flow instabilities during 3D printing based on material extrusion, where the filament is advanced through a melting zone and a nozzle that extrudes the material [7–9]. Zhu et al. [9] observed the shear banding of well-entangled polymer melts during material extrusion under a controlled rate or controlled pressure.

In our previous study [10] on the 3D printability of polymer nanocomposites with carbonaceous fillers, graphene and carbon nanotubes, we explained the flow instability in the printing nozzle as due to the "elastic turbulence" at high Weissenberg numbers and very low Reynolds numbers near to the nozzle walls. However, publications on flow instabilities associated with shear banding and shear slipping during the 3D printing of polymer nanocomposites and how this phenomenon is affected by anisotropic nanofillers are not well studied in the scientific literature. In our latest work [11], we focus on the shear banding model during the rheological measurement of shear stress and afterwards during the material extrusion additive manufacturing process. Thus we assumed that the negative slope of the shear stress in the shear-thinning region is attributed to instability, expressed as banding.

Despite our efforts till now, the main question of what happens with the shear stress during rheological measurements remains open: is there any shear banding or shear slipping, or some other mechanism similar to turbulence, although at a small Reynolds number? Analogous phenomena will also occur in the 3D printing process that manifests shear, as well. In our present survey we try to model the rheological results from experiments of some pure polymers such as polylactide (PLA) and some filled polymer nanocomposites of PLA with graphene nanoplatelets (GNPs) and PLA with multiwall carbon nanotubes (MWCNTs). Since these results show instabilities of shear stress when increasing the shear rate, we apply the three mechanisms, described above, to their corresponding flows in the nozzle region of a 3D printer (considered as a tube).

2 Rheological Models

To determine the rheological behaviour of complex fluids, specific experiments are performed with different types of rheometers: capillary, rotational – cone to plate, parallel plates, etc. During some experiments, flow discontinuity was observed, expressed by a sudden drop in apparent viscosity and shear stress at moderate and high shear rates. At a high Weissenberg number $Wi > 1$ (product of the bulk shear rate and the longest relaxation time), many complex fluids exhibit wall slip and/or shear

banding [12]. Usually, a critical shear stress or shear rate is necessary to cause these discontinuities. Wang, in his review paper [13], suggests that if in case a shear banding occurs as characteristics of entangled polymers, then it is important to understand if it is preceded or accompanied by a wall slip, thus the discontinuity nature of both of them is identical. Afterwards, at higher shear rates, a polymer melt fracture may also occur, which makes further measurements by the rheometer impossible.

As stated by Wang [13] the wall slip and shear banding have the same molecular origin it can be supposed that chain disentanglement is caused by a force imbalance. While at wall slip, the disentanglement starts at the interface between the polymer and wall, the shear banding may start from one monolayer in the bulk, being disentangled first, and then provoking an internal slip. Thus, the wall slip performs like a fast shear band at the interface with a thickness of the order of a monolayer. However, when the shear banding happens away from the interface, it can be easily identified. Sometimes the shear banding appears like a slip (sometimes named apparent wall slip) if it is located at the interface with a thickness much greater than a monolayer, but macroscopically invisible [13].

2.1 Generalized Newtonian model

The registered shear stress during the steady rheological experiments for shear thinning polymers is usually represented as a nonlinear function of the shear rate, $\tau = f(\dot{\gamma})$, from which the viscosity is obtained, $\eta = \tau/\dot{\gamma}$. The viscosity is constant only for the Newtonian fluids, while for non-Newtonian ones the shear stress or viscosity is a nonlinear function of shear rate. This function is often expressed by the generalized Newtonian models, such as the Power law, the Carreau model and its generalization – the Carreau–Yasuda model, the Casson model, the Cross model, etc. [2, 14–23]. In our paper [10] the experimentally registered shear stress $\tau(\dot{\gamma})$ of the nanocomposites is fitted with the Carreau–Yasuda viscosity model:

$$\tau(\dot{\gamma}) = \eta_0(1 + \lambda^a \dot{\gamma}^a)^{(n_c-1)/a}\dot{\gamma}\,, \tag{1}$$

where $\eta_0 = \eta(\dot{\gamma} \to 0)$ is the zero-shear rate viscosity, λ is the relaxation time and n_c is the behavior index. The values of these constants are given in Table 1 for the experimentally studied polymers, PLA and nanocomposites, 1.5% GNP/PLA and 1.5% MWCNT/PLA, and discussed in the present work. It is seen that $n_c < 0$ for all the considered materials, which complicates the modelling with (1) for different flows. In the next Section 3.1, we shall discuss the analytical model of Weissenberg–Rabinowitsch–Mooney (WRM) [24] for the considered here flow in the tube and show that the nonlinearity of (1) gives restrictions to the flow parameters and only for some special cases solutions exist. Otherwise, the general problem can be analyzed only by numerical modelling, as presented in Section 3.2.

Table 1: Values of the constants in (1) and density ρ

Material	η_0 [Pa.s]	λ [s]	n_c	a	ρ [kg/m^3]
PLA	123.4	0.02629	-2.493	2	1240
1.5% GNP/PLA	426.3	0.05149	-5.07	2	1250
1.5% MWCNT/PLA	4712	0.03735	-2.212	0.4963	1250

In Fig. 1 the experimentally registered shear stress of the melt flow at 220°C by a plate-plate rheometer is approximated by eq. (1) with the values of the constants of Table 1. We have to note that the experiments were performed until the shear rate $\dot{\gamma} \leq 100$ s^{-1}, as for larger shear rates in the plate–plate rheometer, the flow starts to oscillate. For better illustration, the shear stress approximated plots are shown also for higher values of $\dot{\gamma} \leq 1000$ s^{-1},

The negative slope of the shear stress is visible for all materials at $\dot{\gamma} > O(1)$, which shows an instability presence of the flow in the rheometer, but not an oscillation. The Weissenberg number for the Carreau-Yasuda model is defined as: $Wi = \lambda\dot{\gamma}_c$, where $\dot{\gamma}_c$ is the critical shear rate found from experiments and given in Table 5 [10]. For higher $\dot{\gamma} > \dot{\gamma}_c$, in the negative slope region, it is evident that $Wi > 1$ and the two following types of instability, discussed below, could be present.

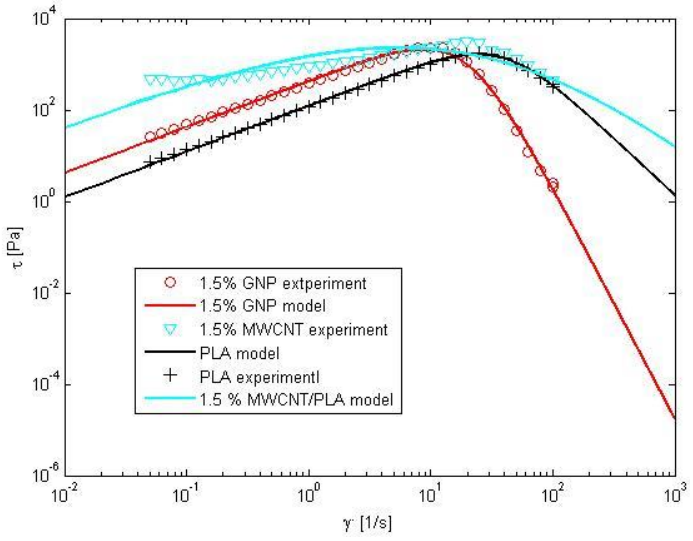

Fig. 1: Experimental data and their approximation with (1) for the shear stress as a function of the shear rate.

2.2 SHEAR SLIP

It is known that wall slip occurs when the stress in the polymeric chains reaches a critical value and eventually leads to permanent detachment from the interface. According to some experimental data [25], the slip velocity, (relative velocity of the fluid with respect to that of the wall), could be regarded as a function of the wall normal and shear stresses, the temperature, the molecular weight and its distribution, the interaction between the fluid and the solid surface and surface roughness. The first model of shear slip was proposed by Navier [26] relating the slip velocity u_m with the wall shear stress τ_w

$$u_{\text{slip}} = \tau_w/\beta\,, \tag{2}$$

where β is the slip coefficient, depending on temperature, normal stress, pressure, molecular parameters surface tension on interface, etc. [25]. The slip coefficient can be given also by $\beta = \eta_w/\delta$, where δ is the extrapolation length (the extrapolated distance from the wall, where velocity would reach zero). Then eq. (2) can be written in terms of this length

$$u_{\text{slip}} = \delta\dot{\gamma}_w \tag{3}$$

with $\dot{\gamma}_w$ as wall shear rate.

For complex fluids, in particular entangled polymers as in our case, this mechanism is more complicated and an insight was made by de Gennes [27], concerning the concept of extrapolation length δ.

In brief, slip can occur at a stress corresponding to the bulk shear rate of the order of the relaxation rate (reciprocal to the terminal relaxation time). We assume that during the measurements in the plate-plate rheometer the polymer melts do not exhibit any slip on both plate walls with serrated surfaces. However during their extrusion in the 3D printer nozzle, we shall concern both cases without slip and with slip on the nozzle wall and a possible length δ will be assessed.

2.3 SHEAR BANDING

A shear banding actually means that the shear rate profile suffers a discontinuity, i.e., the shear rate takes two significantly different values $\dot{\gamma}_1 \leq \dot{\gamma}_c$ and $\dot{\gamma}_2 \gg \dot{\gamma}_c$ when the shear stress is almost the same, here named τ_{band}. This phenomenon is well described in [1] and an example for 1.5% wt. GNP/PLA is given in Fig. 2, where both shear rates $\dot{\gamma}_1$ and $\dot{\gamma}_2$ are denoted, as well as the banding shear stress τ_{band}. For all discussed materials $\dot{\gamma}_1 < 100\ \text{s}^{-1}$, but $\dot{\gamma}_2 > 100\ \text{s}^{-1}$ and is not registered by the experiment. Similarly, as in [11], we extrapolate the shear stress for higher shear

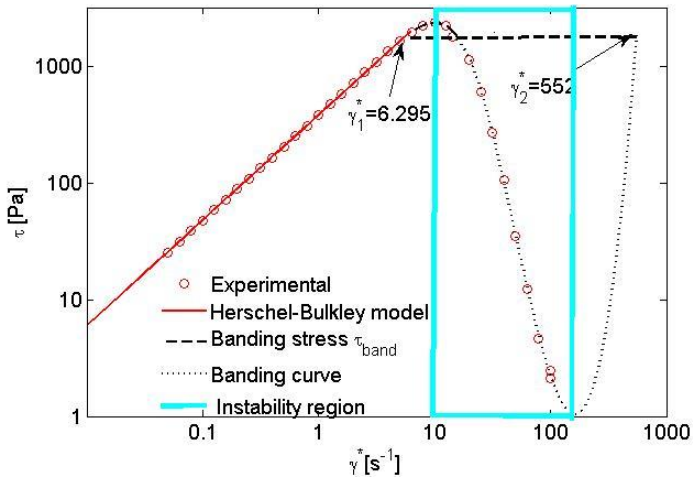

Fig. 2: The shear stress modelling of 1.5 wt.% GNP/PLA. Banding shear stress $\tau_{\text{band}} = \tau(\dot{\gamma}_1) = \tau(\dot{\gamma}_2)$.

rates than 100 s^{-1}. In [28] it is suggested that when the shear rate is in the banding zone the fluid flow is unstable, while at other shear rates above that for which the shear stress is minimal, the flow is predicted either metastable or stable. The unstable flow region between the maximum and minimum shear stress and the corresponding shear rates is marked as a box in Fig. 2.

The rheological behavior of hybrid polymer nanocomposite melts based on PLA filled with MWCNTs and GNPs, approaches the limits of a yield stress fluid, at low shear rates, where the viscosity is very high, and the material behaves as a solid. Therefore in the first stable branch d $\dot{\gamma}<\dot{\gamma}_1$, we use the Herschel–Bulkley model for the shear stress [11, 29]

$$\begin{cases} \dot{\gamma} = 0\,, & \tau \leq \tau_0 \\ \tau = tau_0 + m\dot{\gamma}^n\,, & \tau > \tau_0 \end{cases}, \tag{4}$$

where τ_0 is the yield stress, m and n are constants of the fluid material with dimen-

Table 2: Rheological and banding properties

Material	τ_0 [Pa]	m [Pa.s^n]	n [-]	$\dot{\gamma}_1$ [s^{-1}]	$\dot{\gamma}_2$ [s^{-1}]	τ_{band} [Pa]
PLA	0	118.85	0.9441	12.56	223	1295.85
1.5% GNP/PLA	0	380.19	0.9021	6.295	552	1998.82
1.5% MWCNT/PLA	334.7	511.6	0.6054	9.976	772	2393.9

sions [m] = Pa.s^n and $n = [-]$.

The values of the model constants τ_0, m, n, τ_{band}, $\dot{\gamma}_1$ and $\dot{\gamma}_2$ for the considered materials are given in Table 2.

3 Application to 3D Printing Flow in a Tube (Nozzle)

The 3D printing is based on the material extrusion technics, which consists in a jet flow of the fused polymer from a nozzle on a substrate to produce objects by layer-to-layer deposition. Some nanocomposites experience difficulties during the 3D printing [2], which are connected with the flow instabilities. Moreover, according to our experiments some of the highly filled PLA nanocomposites, with greater than 6% wt. MWCNT in PLA block up the nozzle. Therefore the flow prior to its run out of the nozzle is important to be studied.

Usually during the printing process, which is fully automated with respect to applied pressure (force) at a fixed velocity of filament entry in the printer heating box, only the flow rate of jet exit can be measured. Therefore, the flow modelling in the nozzle is in the fixed flow rate formulation at unknown pressure gradient, i.e., $Q = $ const., for the different cases, as given in Table 3. The nozzle is assumed as a straight tube with radius $R = 0.25$ mm.

Table 3: Flow parameters: flow rate Q, mean velocity U, Reynolds number Re, slip velocity u_{slip} and relative slip coefficient δ/R as calculated in Section 3.1

Material	Q [mm^3/s]	$U = Q/(\pi R^2)$ [mm/s]	$Re = \rho U R/\eta_0$	u_{slip} [mm/s]	δ/R [-]
PLA	1.1723	5.97	1.5 10^{-5}	4.9	0.81
1.5% GNP/PLA	1.2417	6.32	0.46 10^{-5}	5.93	2.75
1.5% MWCNT/PLA	1.2064	6.14	0.04 10^{-5}	5.99	4.43

3.1 Classical Weissenberg–Rabinowitsch–Mooney model

The flow rate formulation will be applied to the fully developed laminar flow through tubes with slip following Weissenberg–Rabinowitsch–Mooney (WRM) theory [24, 30]. The flow rate will be obtained from the wall shear rate in an explicit form instead of directly integrating the velocity over the cross sectional area for Carreau–Yasuda model (1). For the fully developed laminar steady flow of an isothermal and incompressible fluid in infinite tube the equation of motion is simplified to: $\tau(r) = \frac{r}{2}P$, where r is the radial coordinate, x is the axial coordinate, $P = -\frac{dp}{dx}$ is pressure

gradient and the τ is the shear stress. On the tube wall ($r = R$), the shear stress is

$$\tau_w = \tau(R) = \frac{R}{2} P \,. \tag{5}$$

The flow is unidirectional with velocity $u(r)$ and shear rate $\dot\gamma(r) = -\dfrac{du}{dr}$ and wall shear rate is: $\dot\gamma_w = \dfrac{\tau_w}{\eta_w}$, where η_w is obtained from (1) for $\dot\gamma(R) = \dot\gamma_w$. If the flow is with slip, its velocity u_{slip} is given by (2). Then the flow rate function is found as

$$q(r) = \frac{\pi R^2 \tau_w}{\beta} + \pi r^2 u(r) + I_1(r)\,, \quad \text{where} \quad I_1(r) = \frac{\pi R^3}{\tau_w^3} \int\limits_0^{\dot\gamma(r)} \dot\gamma \tau^2(\dot\gamma) \frac{d\tau}{d\dot\gamma} d\dot\gamma \,.$$

At a fixed flow rate Q the wall shear stress τ_w and shear rate $\dot\gamma_w$ must be obtained from the expression for the flow rate in the whole tube

$$Q = q(R) = \frac{\pi R^2 \tau_w}{\beta} + I_1(R)\,, \tag{6}$$

which depends on β [31]. Further, the velocity is found in the integral form

$$u(r) = \left[\frac{I_2(R)}{\pi} - \frac{I_2(r)}{\pi}\right] + \left[\frac{I_1(R)}{\pi} - \frac{I_1(r)}{\pi}\right], \tag{7}$$

where

$$I_2(r) = \frac{2\tau_w^2}{R^2} \int\limits_0^{\dot\gamma(r)} \frac{I_1(\dot\gamma)}{\tau^3(\dot\gamma)} \frac{d\tau}{d\dot\gamma} d\dot\gamma \,.$$

For the Carreau–Yassuda model (1) this integral cannot be obtained analytically, but only after numerical integration. However, $I_1(\dot\gamma(r))$ has the following explicit formula:

$$\begin{aligned} I_1(\dot\gamma) = \frac{\pi R^3}{4(a+4)\tau_w^3} \Bigg\{ & \dot\gamma^4 (a+4)\, {}_2F_1\left(\left[\frac{4}{a}, -\frac{3(n_c-1)}{a}\right], \left[\frac{a+4}{a}\right], -\lambda^a \dot\gamma^a\right) \\ & + 4\lambda^a \dot\gamma^{a+4} (n_c - 1)\, {}_2F_1\left(\left[\frac{a+4}{a}, -\frac{3(n_c-1)+a}{a}\right], \left[\frac{2(a+2)}{a}\right], -\lambda^a \dot\gamma^a\right) \Bigg\}, \end{aligned} \tag{8}$$

where ${}_2F_1$ is the hypergeometrical function. This expression (8) is confirmed at $a = 2$ by the corresponding formula for the Carreau model in [24]. From (6) with (8)

at given β or δ (the extrapolation length or slip coefficient) the wall shear rate $\dot{\gamma}_w$ or stress τ_w is obtained and from (5) — the pressure gradient P.

It occurs that at negative $n_c < 0$, the function $q(\dot{\gamma}(r))$ is of parabolic type for any r. Thus for a fixed value of q, apart from the positive slope $\dfrac{dq(\dot{\gamma})}{d\dot{\gamma}} > 0$, there is a negative slope $\dfrac{dq(\dot{\gamma})}{d\dot{\gamma}} < 0$, which is unrealistic, since the flow inside the tube is an increasing function of $\dot{\gamma}(r)$ and $\dot{\gamma}(r)$ is supposed to reach its maximum on the tube wall. At a fixed flow rate Q, two roots of eq. (6) are found $(\dot{\gamma}_w)_1 \leq (\dot{\gamma}_w)_2$, where the second root corresponds to the negative slope, i.e., unrealistic. Since between the flow rate Q and the pressure gradient P there is a relation expressed by (5) and (6), it occurs that the shear rates corresponding to the positive slope $\dfrac{dq(\dot{\gamma})}{d\dot{\gamma}} > 0$ are identical to those of the slope $\dfrac{d\tau(\dot{\gamma})}{d\dot{\gamma}} > 0$, found from the analysis made on the same problem, but at fixed P and unknown flow rate Q [32].

In Table 3 the values of the minimum slip velocity (corresponding to maximum wall shear rate) are given at minimum possible slip length coefficient (extrapolation length), δ/R for the flow cases given in Table 2. The corresponding velocity profiles are plotted in Fig. 3.

3.2 Numerical model

The negative slope of the shear stress at high shear rate for all nanocomposites is well visible from the experimental data in Fig. 1, which suggests that the pressure is not constant for these shear rates and the WRM model, discussed in the previous section, is not applicable. We expect the flow velocity in the vicinity of the nozzle walls to have a steep slope, which is a result of the strong rheological nonlinearity. Therefore, the full system of Navier–Stokes equations modelling the flow velocity in the nozzle region is solved numerically as in [10]. An iterative procedure in the framework of the software Ansys/Fluent was performed with respect to the index n_c, starting from the Newtonian solution. The flow rate Q (Table 3) was kept constant, the outlet pressure accepted as ambient and no-slip is assumed on the nozzle wall. The velocity profiles for all materials, presented in Fig. 3, were found to be self-similar with a plug flow in almost 90% of the flow region and a boundary layer close to the wall [10].

3.3 Shear banding with shear slipping model

Following [11], we consider an analytical model based on the shear banding and slipping assumption in the same geometry of the nozzle (tube) and flow characteristics given in Table 3. The upper banding limit of the shear rate $\dot{\gamma} = \dot{\gamma}_2$ is supposed

to be reached on the tube wall with $r = R$. For all discussed cases it is seen that $Re \ll 1$, Table 3, which shows that the inertia will not affect the polymer flow and the flow has a complicated character, which is evident from the numerical results in Fig. 3. This confirms the existence of three regions: a yield stress region, $r \leq R_0$; a simple shear region of the tube at $r \leq R_1$; and a boundary region close to the wall with constant banding stress τ_{band}, where R_1 will be obtained from the matching with the flow rate. For the analytical model the flow is sought in these regions as a solution of the following equations of motion:

$$\begin{cases} \dot{\gamma} = 0\,, & \tau_0 \ \text{ at } \ (r \leq R_0)\,, \\ \dfrac{1}{r}\dfrac{d}{dr}(r\tau) = P\,, & \tau_0 < \tau \leq \tau_{\text{band}} \ \text{ at } \ (R_0 < r \leq R_1)\,, \\ \dot{\gamma} = Ar + B\,, & \tau = \tau_{\text{band}} \ \text{ at } \ (R_1 < r \leq R)\,, \end{cases} \tag{9}$$

where P is the pressure gradient, R_0 is the radius of the yield stress region, A and B

$$P = \frac{2\tau_{\text{band}}}{R_1}\,, \qquad R_0 = \frac{\tau_0 R_1}{\tau_{\text{band}}}\,, \qquad A = \frac{\dot{\gamma}_2 - \dot{\gamma}_1}{R - R_1}\,, \qquad B = \dot{\gamma}_2 - AR\,.$$

The velocities corresponding to (3) in the different regions are obtained to be

$$\begin{aligned} u_{\text{yield}} &= u(r = R_0)\,, \\ u &= \frac{n}{n+1}\Big(\frac{P}{2m}\Big)^{\frac{1}{n}}[(R_1 - R_0)^{\frac{1}{n}} - (r - R_0)^{\frac{1}{n}}] \\ u_{\text{band}} &= \frac{A}{2}(r^2 - R^2) + B(r - R) \end{aligned} \tag{10}$$

and the flow rate becomes:

$$W(R_1) = \pi R_0^2 u_{\text{yield}} + 2\pi \int_{R_0}^{R_1} u r dr + 2\pi \int_{R_1}^{R} u_{\text{band}} r dr + \pi R_1^2 u_{\text{band}}(R_1) + \pi R^2 u_{\text{slip}}\,, \tag{11}$$

where $u_{\text{slip}} = \delta\dot{\gamma}_2$ with slip length δ. If there is no slip, $\delta = 0$.

The unknown radius R_1 is obtained when equating the upper expression to the given flow rate Q

$$W(R_1) = Q\,. \tag{12}$$

The profiles of the velocity functions (10) for the considered polymers are presented in Figs. 3a-c, with parameters given in Table 4. These profiles have similar

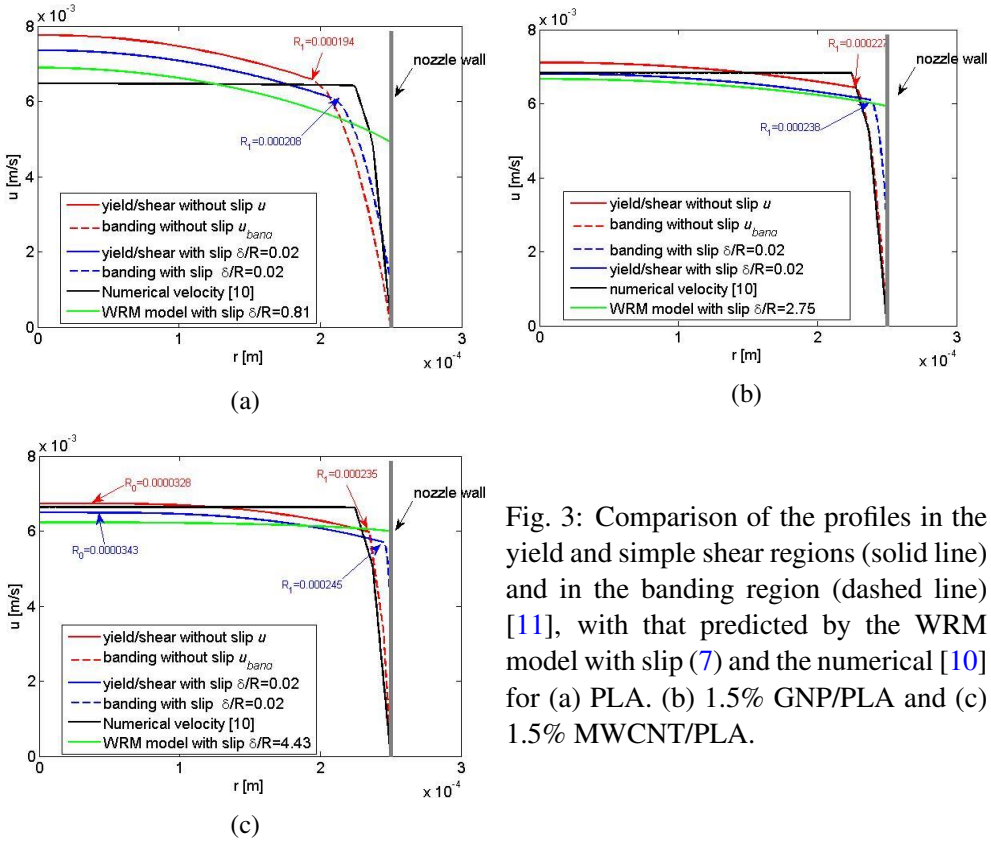

Fig. 3: Comparison of the profiles in the yield and simple shear regions (solid line) and in the banding region (dashed line) [11], with that predicted by the WRM model with slip (7) and the numerical [10] for (a) PLA. (b) 1.5% GNP/PLA and (c) 1.5% MWCNT/PLA.

Table 4: Flow and material parameters in the nozzle without slip/with slip

Material	R_0, R_1 [mm] no slip	R_0, R_1 [mm] slip δ/R =0.02	$Re_{\text{band}} = \dfrac{\rho Q\dot{\gamma}_2}{\pi R\tau_{\text{band}}}$	$Wi_{\text{band}} = \dfrac{\dot{\gamma}_2}{\dot{\gamma}_1}$
PLA	— 0.194	— 0.208	3.2×10^{-4}	17.75
1.5% GNP/PLA	— 0.227	– 0.238	5.4×10^{-4}	87.69
1.5% MWCNT/PLA	0.033 0.235	0.034 0.245	6.2×10^{-4}	77.35

forms as those obtained from the numerical model given in [10]. Since the pressure is not constant, $P_{\text{band}} = 2\tau_{\text{band}}/r$ in the banding region, vortices may exist in it, giving rise to turbulent structures, as discussed in [10]. The material with yield stress has a

pronounced plug flow, Fig. 3c. For PLA from Figure 3a, the parabolic velocity profile spreads on a larger zone in the tube, which resembles in some sense the Poiseuille profile of Newtonian fluids. This is connected with its $\dot{\gamma}_1$, which has the highest value among the all considered materials (Table 2). The Reynolds number Re_{band} and Weissenberg number Wi_{band} for the banding region are also given in Table 4. The very high Wi_{band} confirms the flow instability in the banding region.

4 Conclusions

In the present study, three different ways to model the instability of shear stress of shear thinning polymers during their rheological measurement in plate-plate rheometer are applied. The experimental data of shear stress have complicated structure with positive and negative slopes and are approximated in the following manner: 1) as a nonlinear function of shear rate by a generalized Newtonian model, e.g. Carreau-Yasuda model; 2) by a wall shear slip using the Navier linear model; 3) as shear banding with yield, e.g. Herschel–Bulkley model. These models are used for three different materials: pure poly(lactic) acid (PLA), poly(lactic) acid (PLA) nanocomposite filled with 1.5% wt. graphene nanoplatelets (GNP) and poly(lactic) acid (PLA) nanocomposite filled with 1.5% wt. multiwall carbon nanotubes (MWCNT). Among the three studied materials only the MWCNT-based nanocomposite exhibits yield at this low filler content.

The three rheological models are applied for the flow of these materials in the nozzle tube of the 3D printer. Since during the extrusion process, only the flow rate can be measured, while the pressure gradient is unknown, the flow rate formulation is applied to the fully developed laminar flow through tubes with slip, as in the Weissenberg–Rabinowitsch–Mooney (WRM) theory. This analytical model is valid only for the positive slope of flow rate with shear rate. Explicit formulas are found for the flow rate and velocity, while the wall shear rate and stress are obtained from the value of the flow rate. It occurs that for the experimentally registered flow rates, the existing flows are only with wall slip. Therefore, for the whole shear stress range, the flow is solved numerically by an iterative procedure based on the software Ansys/Fluent for the nozzle region. The numerical simulation of the flow in the boundary layer shows that the combination of the high Weissenberg number and the very low Reynolds number causes “elastic turbulence” with a plug flow, which could hamper the jet flow from the nozzle or even produce clogging [10]. Another analytical model for shear stress with banding is proposed for the flow in the nozzle considering the flow region composed of three different regions in the tube, which match on their boundaries. This model has an advantage over the upper numerical model, as it explains the structure of the flow in the nozzle tube and makes it possible to conclude which materials are easier or harder to print [11]. The experimental rhe-

ology supported with a simple analytical model for shear stress with banding explains the role of flow instability in the 3D printing process.

ACKNOWLEGEMENTS

S.T. acknowledgement: "I would like to express my enormous gratitude to my teacher and advisor - Prof. Zapryan Zapryanov, who opened me to the fascinating world of Fluid mechanics from my early years as his master's and PhD student for my whole life."

R.K. acknowledges the support from H2020-FET-Graphene Flagship-881603-Core 3 and BG05M2OP001-1.001-0008 National Center on Mechatronics and Clean Technologies.

REFERENCES

[1] T. DIVOUX, M.A. FARDIN, S. MANNEVILLE, S. LEROUGE (2016) Shear Banding of Complex Fluids. *Annual Review of Fluid Mechanics* **48** 81-103.

[2] S.M. FIELDING, P.D. OLMSTED (2004) Spatiotemporal Oscillations and Rheochaos in a Simple Model of Shear Banding. *Physical Review Letters* **92** 084502.

[3] P.E. BOUKANY, S.Q. WANG (2009) Exploring the Transition from Wall Slip to Bulk Shearing Banding in Well Entangled DNA Solutions. *Soft Matter* **5** 780-789.

[4] J.L. GOVEAS, G.H. FREDRICKSON (1999) Curvature-Driven Shear Banding in Polymer Melts. *Journal of Rheology* **43** 1261-1277.

[5] S. LEROUGE, P.D. OLMSTED (2020) Non-Local Effects in Shear Banding of Polymeric Flows. *Frontiers of Physics* **7** 246.

[6] Y.T. HU, C. PALLA, A. LIPS (2008) Comparison between Shear Banding and Shear Thinning in Entangled Micellar Solutions. *Journal of Rheology* **52** 379.

[7] M.E. MACKAY (2018) The Importance of Rheological Behavior in the Additive Manufacturing Technique Material Extrusion. *Journal of Rheology* **62** 1549.

[8] M.P. SERDECZNY, R. COMMINAL, D.B. PEDERSEN, J. SPANGENBERG (2020) Experimental and Analytical Study of the Polymer Melt Flow through the Hot-End in Material Extrusion Additive Manufacturing. *Additive Manufacturing* **32** 100997.

[9] X. ZHU, W. YANG, S.-Q. WANG (2013) Exploring Shear Yielding and Strain Localization at the Die Entry during Extrusion of Entangled Melts. *Journal of Rheology* **57** 349-364.

[10] R. KOTSILKOVA, S. TABAKOVA, R. IVANOVA (2022) Effect of Graphene Nanoplatelets and Multiwalled Carbon Nanotubes on the Viscous and Viscoelastic Properties and Printability of Polylactide Nanocomposites. *Mechanics of Time-Dependent Materials* **26** 611-632.

[11] R. KOTSILKOVA, S. TABAKOVA (2023) Exploring Effects of Graphene and Carbon Nanotubes on Rheology and Flow Instability for Designing Printable Polymer Nanocomposites. *Nanomaterials* **13**(5) 835.

[12] P.E. BOUKANY, S.Q. WANG, S. RAVINDRANATH, L.J. LEE (2015) Shear Banding in Entangled Polymers in the Micron Scale Gap: A Confocal-Rheoscopic Study. *Soft Matter* **11** 8058.

[13] S.Q. WANG (2019) From Wall Slip to Bulk Shear Banding in Entangled Polymer Solutions. *Macromolecular Chemistry and Physics.* **220**(1) 1800327.

[14] R.B. BIRD, R.C. ARMSTRONG, O. HASSAGER (1987) "Dynamics of Polymeric Liquids", 2nd Edition, Vol. 1. Wiley, New York.

[15] P.R. CHHABRA, J.F. RICHARDSON (2008) "Non-Newtonian Flow and Applied Rheology: Engineering Applications". Cambridge University Press, Cambridge.

[16] T.J. COOGAN, D.O. KAZMER (2019) In-Line Rheological Monitoring of Fused Deposition Modeling. *Journal of Rheology* **63** 141-155.

[17] B.S. BALANI, F. CHABERT, V. NASSIET, A. CANTAREL (2019) Influence of Printing Parameters on the Stability of Deposited Beads in Fused Filament Fabrication of Poly(Lactic) Acid. *Additive Manufacturing* **25** 112-121.

[18] B.S. BERAN, T. MULHOLLAND, F. HENNING, N. RUDOLPH, T.A. OSSWALD (2018) Nozzle Clogging Factors During Fused Filament Fabrication of Spherical Particle Filled Polymers. *Additive Manufacturing* **23** 206-214.

[19] V. NIENHAUS, K. SMITH, D. SPIEHL, E. DÖRSAM (2019) Investigations on Nozzle Geometry in Fused Filament Fabrication. *Additive Manufacturing* **28** 711-718.

[20] F. PIGEONNEAU, D. XU, M. VINCENT, J.-F. AGASSANT (2020) Heating and Flow Computations of an Amorphous Polymer in the Liquefier of a Material Extrusion 3D Printer. *Additive Manufacturing* **32** 101001.

[21] J.L.C. QUINTANA, S. HIEMER, N.G. DUARTE, T. OSSWALD (2021) Implementation of Shear Thinning Behavior in the Fused Filament Fabrication Melting Model: Analytical Solution and Experimental Validation. *Additive Manufacturing* **37** 101687.

[22] D.D. PHAN, J.S. HORNER, Z.R. SWAIN, A.N. BERIS, M.E. MACKAY (2020) Computational Fluid Dynamics Simulation of the Melting Process in the Fused Filament Fabrication Additive Manufacturing Technique. *Additive Manufacturing* **33** 101161.

[23] S.K. KIM, D.O. KAZMER, A.R. COLON, T.J. COOGAN, A.M. PETERSON (2021) Non-Newtonian modeling of contact pressure in fused filament fabrication. *Journal of Rheology* **65** 27-42.

[24] S.K. KIM (2018) Flow-Rate Based Method for Velocity of Fully Developed Laminar Flow in Tubes. *Journal of Rheology* **62** 1397-1407; Erratum (2021) *Journal of Rheology* **65** 289.

[25] M.M. DENN (2001) Extrusion Instabilities and Wall Slip, *Annual Review of Fluid Mechanics* **33** 265-287.

[26] C.L.M.H. NAVIER (1827) Sur Les Lois de Mouvement des Fluides, *Mémoires de l'Academie Royale des Sciences de l'Institut de France* **6** 289-440.

[27] F. BROCHARD, P.G. DE GENNES (1992) Shear-Dependent Slippage at a Polymer/Solid Interface. *Langmuir* **8** 3033-3037.

[28] C. GRAND, J. ARRAULT, M.E. CATES (1997) Slow Transients and Metastability in Wormlike Micelle Rheology. *Journal of Physics B: Atomic and Molecular Physics*. **7** 1071-1086.

[29] G.C. GEORGIOU (2021) Simple Shear Flow of a Herschel-Bulkley Fluid with Wall Slip above a Threshold Stress. *Applications in Engineering Science* **8** 00068.

[30] T. SOCHI (2015) Analytical Solutions for the Flow of Carreau and Cross Fluids in Circular Tubes and Thin Slits. *Rheologica Acta* **54** (8) 745-756.

[31] G. KAOULLAS, G.C. GEORGIOU (2013) Newtonian Poiseuille flows with Slip and Non-Zero Slip Yield Stress. *Journal of Non-Newtonian Fluid Mechanics* **197** 24-30.

[32] N. KUTEV, S. TABAKOVA (2023) A Note on the Steady Poiseuille Flow of Carreau–Yasuda Fluid. In: Slavova, A. (eds)"New Trends in the Applications of Differential Equations in Sciences (NTADES 2022)". *Springer Proceedings in Mathematics & Statistics* **412** 105-115. Springer, Cham.